Article:
Drougkas, A orcid.org/0000-0002-8647-9993, Esposito, R, Messali, F et al. (1 more author) (2021) Analytical Models to Determine In-Plane Damage Initiation and Force Capacity of Masonry Walls with Openings. Journal of Engineering Mechanics, 147 (11). 04021088. ISSN 0733-9399

https://doi.org/10.1061/(asce)em.1943-7889.0001995

Analytical models to determine in-plane damage initiation and force capacity of masonry walls with openings

Anastasios Drougkas[1], Rita Esposito, Francesco Messali

Faculty of Civil Engineering and Geosciences, TU Delft, Stevinweg 1, 2628 CN, Delft, The Netherlands

Vasilis Sarhosis

School of Civil Engineering, University of Leeds, Woodhouse Lane, LS2 9JT, Leeds, United Kingdom

Abstract

Masonry panels consisting of piers and spandrels in buildings are vulnerable to in-plane actions caused by seismicity and soil subsidence. Tectonic seismicity can be hazardous for the safety of masonry structures, whereas low-magnitude induced seismicity can be detrimental to their durability due to the accumulation of light damage. This is particularly true in the case of unreinforced masonry. Therefore, the development of models for the accurate prediction of both damage initiation and ultimate capacity for masonry elements and structures is necessary.

In this paper a method based on analytical modelling for the prediction of the damage initiation mode and capacity of stand-alone masonry piers is presented, followed by the expansion of the model through a modular approach to masonry walls with asymmetric openings. The models account for all potential damage and failure modes for in-plane loaded walls.

The stand-alone piers model is applicable to all types of masonry construction. The wall with openings model can be applied as-is to simple buildings but can also be extended to more complex structures with simple modifications. The model results are compared with numerous experimental cases and exhibit very good accuracy.

[1] Corresponding author: A.Drougkas@tudelft.nl

Keywords

masonry – earthquake engineering – analytical modelling – limit analysis – in-plane loading

Notation

h	height
h_0	effective height
l	length
t	thickness
m	width of compressive stress fan at centre-height
b	width of compression strut
f_c	compressive strength of masonry
f_t	tensile strength of masonry
f_v	initial shear strength (cohesion)
μ	friction coefficient (tangent of friction angle)
σ	vertical stress
τ	shear stress
V	vertical force
H	horizontal force

Highlights

- Closed-form expressions predict the damage initiation mode and capacity of piers
- Analytical modelling predicts the in-plane shear capacity of masonry walls with openings
- The models are accurate against newly elaborated and existing experimental data

1 Introduction

1.1 State of the art

Masonry structures are vulnerable to seismic loading due to their low tensile and shear strength. While out-of-plane effects can be severely detrimental to the safety of masonry structures, these are often offset when adequate connections allow for the force distribution to the transversal walls via floor diaphragm action. Even if such measures are taken, in-plane failure remains a problem to deal with.

Typically, four main failure modes may be clearly distinguished: a) rocking, b) sliding, c) biaxial failure and d) compressive failure. These failure modes, listed in order of appearance under increasing levels of applied vertical stress, define, in combination, a failure envelope for masonry piers under in-plane shear.

Rocking mode failure arises due to the very low tensile strength of masonry perpendicularly to the bed joints, leading to a clear localisation of the bending crack. Models for the rocking capacity can be easily derived through simple equilibrium in bending [1,2]. Other models have been proposed in design codes [3]. Sliding due to shear, typically localised in bed joints is often described using a Mohr-Coulomb failure criterion. Expressions to determine the capacity in shear at the scale of structural member have been proposed in the literature [1,4] and used in design codes [5]. Models for diagonal failure are generally more complex due to the interaction of compression and tension in an area of the pier that is not as clearly defined as in rocking or sliding. Several models for biaxial failure have been proposed in the literature [6–8], each with different considerations for the dimensions of the pier and the mechanical properties of the masonry composite.

The formulation of models for the prediction of the force capacity of masonry walls with openings is complicated by the frame action made possible by the spandrels, whose failure needs to be accounted for [9]. Simple analytical models accounting for the interaction of failure modes of piers and spandrels in walls with openings are currently lacking in the literature.

The available experimental inventory on masonry stand-alone piers subjected to in-plane shear under vertical stress is extensive [10], and continuously updated [11]. It includes masonry composites made of different materials, with widely different dimensions and aspect ratios, different boundary conditions and

in different bond types. Experimental tests on masonry walls with windows or openings, accompanied by a characterization of the mechanical properties of the masonry composite, are less frequent and feature a smaller variety of boundary conditions [12–16].

In addition to capacity calculation, the complications introduced by induced seismicity raise the issue of correctly identifying the mode of damage initiation in masonry structures. Combined soil subsidence and low-magnitude seismicity have been shown to impose mostly in-plane demands on masonry structures [17–19]. These demands are the source of light damage, linked to damage initiation rather than collapse.

Upper-bound approaches for the calculation of the capacity of masonry walls with openings have been proposed in the literature. However, a simple model with general applicability for the prediction of the force capacity of masonry walls with openings, one based on the material properties of the masonry composite, is still lacking. Such a model should allow a quick calculation of the capacity of a masonry structure, the prediction of the critical failure mode and the evaluation of the influence of structural intervention on the behaviour without resorting to complex finite element or macro-element modelling.

Furthermore, a simple model for the identification of the in-plane damage initiation mode of masonry piers has not been yet proposed. The need of such a model arises from the increase in low-magnitude induced seismicity near urban centres, which does not necessarily raise the risk of collapse but may be the cause of light damage in masonry structures [16]. A-priori knowledge of the location of damage initiation using simple approaches allows the application of targeted intervention at vulnerable areas. Further, such a model can prove useful as a structural inspection tool, assisting in focusing damage mapping efforts in existing masonry buildings on the areas where damage is expected to arise.

1.2 Objectives

The primary objective of the present paper is the presentation of a simple model for the calculation of the in-plane shear capacity of masonry structures. In the context of the paper, the term masonry structure refers to walls with door- or window-openings, in essence masonry portal frames with or without a base spandrel. The model should account for frame action afforded by the spandrel, whose contribution is itself

limited by potential damage. Through a modular approach, this model is applicable to masonry elements with multiple openings.

The secondary objective of the paper is the development of a simple model for the prediction of the damage initiation mode in masonry piers subjected to in-plane shear. Essentially, this model should be able to predict the failure mode that arises first in masonry piers under shear. Such a model can be used in stand-alone piers or can be alternatively plugged-in to the proposed model for masonry structures.

The development of the masonry structure model is based on the assembly and evaluation of simple models predicting the capacity of piers in well-defined failure modes. A new model for the biaxial failure of masonry is here proposed. These models define a capacity envelope. The results of the failure models are compared to numerous experimental results from the literature on stand-alone piers.

Moving beyond the application of these models in stand-alone piers, the paper presents a method of application to complex walls with openings, dealing with issues of force distribution and the development of admissible failure modes depending on boundary conditions. This model is validated against case studies from the literature, limiting the investigation to cases where a comprehensive determination of the mechanical properties of the masonry composite is available.

The damage initiation model is developed along the lines of a proposed envelope, similarly to the model for the capacity of piers. A comparison with the corresponding capacity envelope is provided.

2 Analytical force capacity models for piers

2.1 Overview

The dimensions of the pier are $l \times h \times t$ (length × height × thickness). For a given masonry compressive strength f_c and a vertical applied stress σ (negative for compression), the length of the compressed toe b_r, assuming a constant rectangular distribution of vertical stress, or b_t, assuming a triangular distribution, is:

$$b_r = -\frac{\sigma}{f_c} l$$
$$b_t = -2\frac{\sigma}{f_c} l \tag{1}$$

For a given set of geometric and material parameters of a stand-alone pier, the applied vertical force V and the horizontal force capacity H are calculated as:

$$V = l \cdot t \cdot \sigma$$
$$H = l \cdot t \cdot \tau \tag{2}$$

The shear stress capacity τ is calculated for each of the considered failure modes below. An envelope curve of the capacity can be drawn by varying σ in the range $[0, f_c]$ and considering the minimum value of τ obtained between the considered failure modes. The considered failure modes are illustrated in Figure 1.

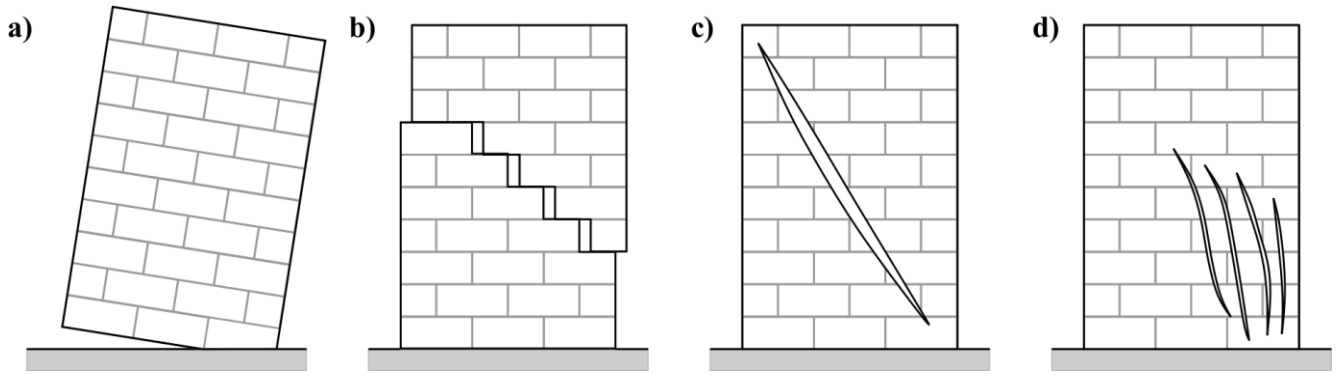

Figure 1 Pier failure modes: a) bending, b) shear, c) biaxial tension-compression and d) compression.

The pier is always considered clamped at the base and may be in a cantilever or double-clamped configuration when rotational restraint is provided. The boundary condition at the top determines the effective height h_0 of the pier, with $h_0 = 1.0$ for a cantilever and $h_0 = 0.50$ for a double-clamped configuration.

2.2 Rocking mode capacity

In a cantilever configuration, the vertical force V is applied at the centre of the top of the pier, while in a clamped top configuration it is applied at a distance of $b_r/2$ from the edge. The compression strut extends

from the point of application of V to the centre of the compressed toe. Through equilibrium of forces and moments, the capacity of a cantilever pier in rocking is:

$$\tau = -\sigma\left(\frac{l}{2} - \frac{b_r}{2}\right)/h \tag{3}$$

while for a clamped top the capacity is:

$$\tau = -\sigma\,(l - b_r)/h \tag{4}$$

In a more general formulation, the horizontal force capacity H can be expressed as the horizontal component of a force acting between two points at a horizontal distance of l and a vertical distance of h whose vertical component is equal to V:

$$H = V\frac{l}{h} \tag{5}$$

2.3 Shear mode capacity

For the shear capacity of the pier, the model proposed by Magenes and Calvi is used [1]. In the notation of the present paper, the shear capacity is equal to:

$$\tau = \frac{f_v - \mu \cdot \sigma}{1 + h_0/l} \tag{6}$$

where f_v is the initial shear strength (cohesion) and μ is the friction coefficient (tangent of friction angle). As noted in the cited work, these parameters are meant to be understood as globally representing the shear characteristics of the masonry composite rather than that of the bed joints.

2.4 Biaxial mode capacity

A new approach based on principal stresses is proposed for calculating the capacity of the pier against biaxial failure. For the interaction of tension and compression, a simple linear failure criterion in planar stress is adopted:

$$f = \frac{\sigma_1}{f_t} - \frac{\sigma_2}{f_c} - 1 \tag{7}$$

where σ_1 is the maximum principal stress (tensile), σ_2 is the minimum principal stress (compressive) and f_t is the tensile strength of the masonry composite. This failure criterion clearly describes the interaction of tensile and compressive stresses in quasi-brittle materials with a shape approximating very closely a linear Mohr-Coulomb criterion.

The compressive stress distribution in a cantilever pier is considered to assume a fan shape, extending along the entire length l of the wall at the top and contracting to the width of the compressive strut b_t at the base. A depiction of this fan shape is illustrated in Figure 2a. The width of the fan m at centre height, where diagonal cracking typically originates, is:

$$m = \frac{l + b_t}{2} \tag{8}$$

In double-clamped piers, the stress fan assumes the shape shown in Figure 2b, with a laterally expanding branch from top to mid-height and a contracting branch from mid-height to base. The angle θ_e of the right external line of the fan with respect to the vertical is limited by the shear strength characteristics of the masonry composite [2]. Considering that the vertical stress at the edge of the fan is zero, the limit values for the tangent of this angle is:

$$\tan(\theta_e - \theta_c) \leq \mu \tag{9}$$

where θ_c in the angle of the line connecting the centres of the strut edges with respect to the vertical. In this context, the friction coefficient of masonry does not coincide with the friction coefficient of the unit-mortar interface. It is a parameter related to the masonry geometric bond and the resulting interlocking of units, with a minimum value equal to the friction coefficient of the unit-mortar interface. As such, for running bond masonry this coefficient is equal to $\mu = (l_u/2)/(h_u + h_m)$, for Flemish bond it is equal to $\mu = (3\, l_u/4)/(h_u + h_m)$ and for English bond it is $\mu = (l_u/2)/(2h_u + 2h_m)$ with l_u, h_u and h_m being the length of the unit, height of the unit and height of the mortar bed joint respectively. The accuracy of this calculation of the friction coefficient is increased with the increase of the size of the masonry member, due to the clearer formation of diagonal cracks following the masonry bond. The maximum length for m is only limited by the length of the pier.

Based on these conditions, the width m of the fan at centre height of a double-clamped pier is:

$$m = b_t + \min\left[l - b_t, \frac{h}{2}\mu\right] \tag{10}$$

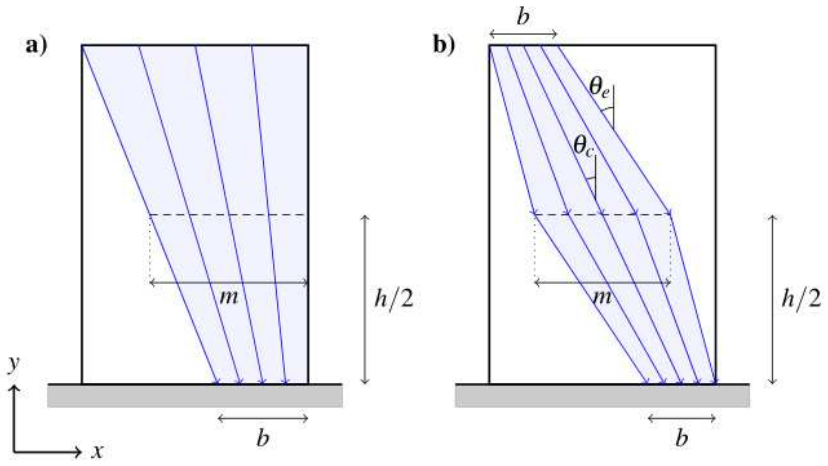

Figure 2 Distribution of compressive stresses in stand-alone pier for biaxial mode evaluation: a) cantilever pier, b) double-clamped pier.

For the orthogonal stress state at the mid-height, it is assumed that the horizontal σ_x stress is zero and that the vertical stress σ_y is evenly distributed. Therefore, it follows that:

$$\begin{aligned} \sigma_x &= 0 \\ \sigma_y &= \sigma\frac{l}{m} \end{aligned} \tag{11}$$

According to Mohr's circle [20], the average stress σ_m is:

$$\sigma_m = \frac{\sigma_x + \sigma_y}{2} \tag{12}$$

and, in combination with the adopted failure criterion according to eq. (7), the principal stresses are:

$$\begin{aligned} \sigma_1 &= \frac{2f_t\sigma_m + f_c f_t}{f_t + f_c} \\ \sigma_2 &= \frac{2f_c\sigma_m - f_c f_t}{f_t + f_c} \end{aligned} \tag{13}$$

The radius of Mohr's circle R is:

$$R = \frac{\sigma_1 - \sigma_2}{2} \tag{14}$$

and the resulting shear stress τ_m is:

$$\tau_m = \sqrt{R^2 - {\sigma_m}^2} \tag{15}$$

This shear stress τ_m acts along the length m of the fan at the evaluated position. Therefore, the equivalent stress τ along the length l of the pier is:

$$\tau = \tau_m \frac{m}{l} \tag{16}$$

The determination of the uniaxial horizontal tensile strength of masonry f_t is a complicated issue. It is a function of the tensile strength $f_{t,u}$ of the units, the tensile strength $f_{t,m}$ of the mortar, the tensile strength $f_{t,i}$ of the unit-mortar interface and the shear strength $f_{v,b}$ of the bed joints. While for masonry in regular bond pattern the vertical tensile strength may be taken as the tensile strength of the unit-mortar interface, the staggered arrangement of the units in, for example, running bond, complicates the failure mechanism. A simple model for the horizontal tensile strength of masonry is therefore introduced. It is based on the identification of three failure modes for the masonry composite in horizontal tension: a) tensile failure of the upper head joint unit-mortar interface together with shearing of the bed joint along the length of half a unit and tensile failure of the lower head joint unit-mortar interface, b) tensile failure of the upper head joint unit-mortar interface together with tensile failure of the bed joint and tensile failure of the lower unit, c) tensile failure of the upper unit together with tensile failure of the bed joint and tensile failure of the lower unit. These modes are illustrated in Figure 3 and are expressed analytically as:

$$\begin{aligned} f_{t,a} &= \frac{f_{t,i}\frac{h_u}{2} + f_{v,b} l_o + f_{t,i}\frac{h_u}{2}}{h_u + h_m} \\ f_{t,b} &= \frac{f_{t,i}\frac{h_u}{2} + f_{t,m} h_m + f_{t,u}\frac{h_u}{2}}{h_u + h_m} \\ f_{t,c} &= \frac{f_{t,u}\frac{h_u}{2} + f_{t,m} h_m + f_{t,u}\frac{h_u}{2}}{h_u + h_m} \end{aligned} \tag{17}$$

$$f_t = min[f_{t,a}, f_{t,b}, f_{t,c}]$$

where l_o is the overlap length between the beds of the units which contributes to the shear mechanism. This length can be easily determined for the most common masonry bonds. For running bond it is equal to $l_u/2$, for Flemish and English bond it is equal to $l_u/4$ and in stack bond it is equal to 0. In addition to regular masonry with mortared joints, eq. (17) can account for dry masonry through the contribution of $f_{v,b}$ and for masonry with unfilled head joints by considering $f_{t,i} = 0$.

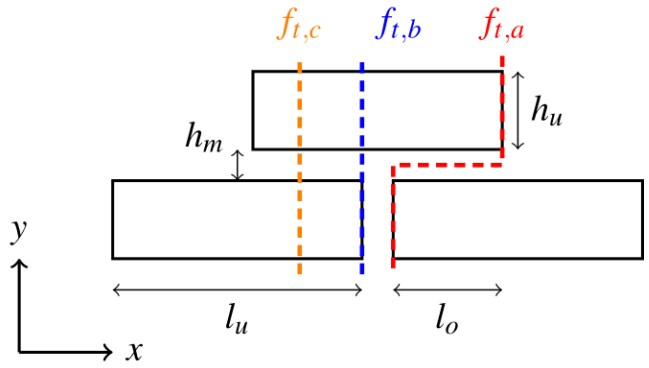

Figure 3 Illustration of potential horizontal tensile failure modes for masonry. Planes of failure for each mode indicated in dashed lines.

2.5 Compression mode capacity

The capacity of the pier in compression is calculated through a simple superposition of the normal stresses at the base of the pier due to the applied vertical stress σ and the bending moment caused by τ applied at the top of the pier. Limiting the minimum stress to the compressive strength $-f_c$, the shear capacity is equal to:

$$\tau = \frac{(l - b_r)}{6h} f_c \tag{18}$$

2.6 Model results and validation

All failure models yield non-negative results for $\sigma \in [0, f_c]$ and produce a capacity envelope as qualitatively shown in Figure 4 for a cantilever pier, defined by the minimum value among the models for a given value of σ. In the case of a clamped pier, the τ envelope is altered only in the region of low vertical stress σ, as both rocking and shear capacity increase. This results in an increase in the range of biaxial

failure towards the range of lower vertical stress σ. This shift is critical given that most masonry piers, due to their large dimensions, function at a relatively low level of average vertical stress from self-weight and service loads in buildings.

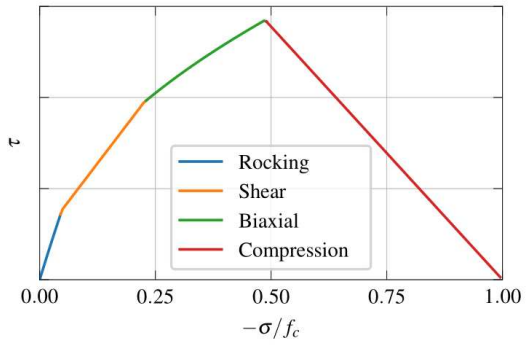

Figure 4 Capacity envelope for piers, derived from the four considered failure modes.

The results of the model combination are tested against the dataset of experimental results assembled by Morandi et al [10]. The dataset includes 188 experimental results of masonry piers subjected to in-plane shear under vertical stress. Material properties are included in the dataset. However, this data is not always fully reported. In the absence of a reported tensile strength f_t this was calculated according to eq. (17). A conservative value of 0.100 $\mathrm{N/mm^2}$ was assumed for $f_{t,i}$ in masonry with mortared head joints, and the tensile strength of the mortar and units was taken as 10% of their respective compressive strengths [21]. Rather than assigning nominal values, the cases where f_v or μ where not reported were disregarded. This filtering resulted in 36 cases with reported f_t and 27 cases with no reported f_t to be considered for analysis, for a total of 63 cases, that is 33% of all reported cases in the cited dataset.

The results of the comparison are plotted in Figure 5. When relying on the reported f_t (Figure 5a) the obtained coefficient of determination R^2 is 0.955 and the mean percentage error MPE is -9.55%, indicating excellent global agreement between the experimental data and analysis results and a tendency of the model to underestimate the capacity. The proposed envelope rarely overestimates the capacity of the piers by more than 15%. The accuracy of the model is noticeably increased when not relying on the reported f_t (Figure 5b) but rather by relying only on the f_t as calculated using eq. (17). The obtained R^2 is slightly increased to 0.962 and the MPE is increased to -5.42%, indicating an enhancement of the model's accuracy,

especially in the cases with higher capacity. This improvement validates the accuracy of the proposed model for the tensile strength of masonry and the calculated biaxial failure envelope. Due to the accuracy of the obtained results, the envelope described by these failure models is considered appropriate for application in the analysis of more complex wall structures.

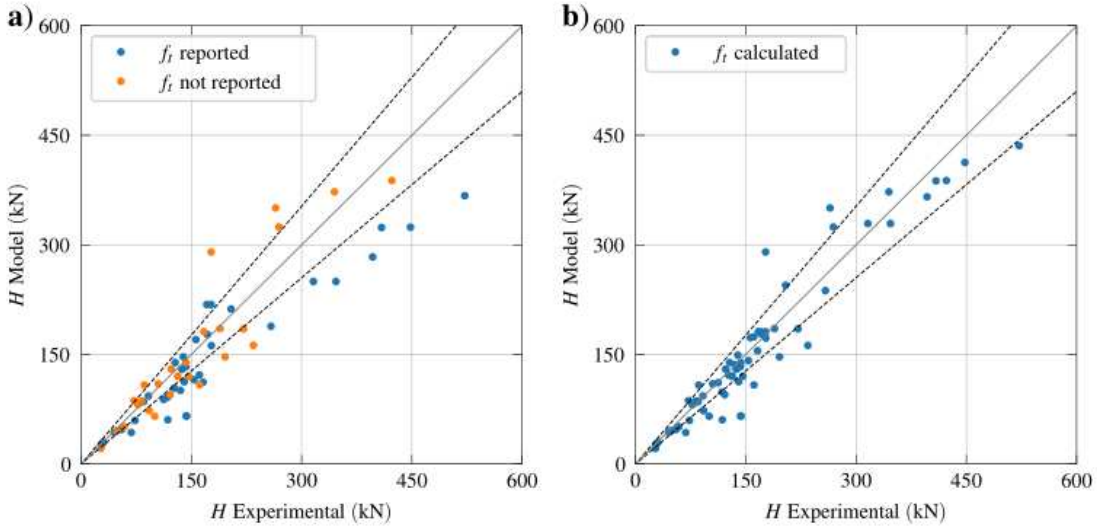

Figure 5 Results of pier capacity model against dataset of experimental data [10]**: a) relying on the reported f_t, b) relying only on calculated f_t. Dashed lines indicate 15% difference, solid line marks equality.**

3 Analytical damage initiation models for piers

3.1 Overview

The proposed damage initiation model for stand-alone piers functions similarly to the capacity model. However, instead of calculating the peak shear force for a specific failure type, it calculates the shear force activating a specific failure type. It may, therefore, be used for identifying the sequence of damage mode initiation and propagation in stand-alone piers loaded in-plane.

Under the assumption that the pier is uncracked before damage initiation, the normal stresses can be easily computed through superposition of the stresses due to σ and τ applied at the top of the pier. Similarly, the distribution of shear stress along the length of the pier assumes a parabolic shape, with the maximum shear stress being 1.5 times the average [22].

3.2 Rocking mode initiation

Damage initiation in rocking occurs under the following conditions: a) a constant vertical stress distribution at the top and a triangular vertical stress distribution at the base are assumed, b) for the maximum stress at the least compressed toe: $\sigma_{max} = f_{t,i}$, c) for the minimum stress at the compressed toe: $\sigma_{min} \geq -f_c$.

According to moment and force equilibrium, and based on the above conditions, the resulting value for the damage initiation shear stress is:

$$\tau = \left(f_{t,i} - \sigma\right)\frac{l}{6h} \tag{19}$$

3.3 Shear mode initiation

The conditions for shear mode initiation are: a) a trapezoidal vertical stress distribution is assumed at the base, b) for the maximum stress at the least compressed toe: $\sigma_{max} \leq f_{t,i}$, c) for the minimum stress at the compressed toe: $\sigma_{min} \geq -f_c$, d) the maximum shear stress due to the trapezoidal distribution needs to reach the shear strength. Therefore, $\tau = (f_v - \mu \cdot \sigma_{max})/1.5$.

Based on these assumptions and applying moment equilibrium, the values for the minimum and maximum stress are:

$$\sigma_{max} = \frac{f_v \cdot h - (2 \cdot \mu \cdot h + l)\sigma}{h \cdot \mu + l} \tag{20}$$

$$\sigma_{min} = -\frac{l \cdot \sigma + 4 \cdot f_v \cdot h}{4 \cdot h \cdot \mu + l}$$

while the value for the damage initiation shear stress is:

$$\tau = 2\frac{f_v - \sigma \cdot \mu}{12 \cdot h \cdot \mu + 3 \cdot l}l \tag{21}$$

3.4 Biaxial mode initiation

The biaxial mode initiation stress is calculated similarly to the capacity according to eq. (8) through eq. (16). Due to the assumption that no other damage initiation mode has arisen, the pier remains uncracked

and the stress fan is vertical, the horizontal force being resisted by friction. Therefore, the width of the fan m is equal to the length of the pier l. Due to the parabolic shear stress distribution along the length of the pier, the damage initiation shear stress is equal to:

$$\tau = \frac{\tau_m}{1.5} \tag{22}$$

3.5 Model results and validation

The three mode initiation models can be combined to produce a damage initiation envelope. This envelope is additionally delimited by the compressive failure model as defined in eq. (18). The brittleness of the compressive failure mode results in the coincidence of damage initiation and ultimate capacity load. Plotting the damage initiation envelope for a masonry pier results in a typical curve shown in Figure 6, where a comparison with the capacity envelope is shown. The damage initiation envelope is always below the capacity envelope.

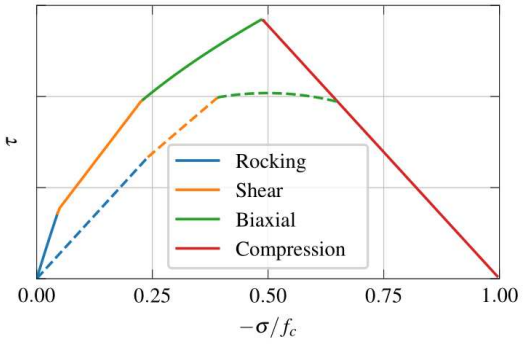

Figure 6 Damage initiation model envelope for piers, derived from the four considered damage initiation modes in dotted lines. Capacity envelope in solid lines.

The range of normalised vertical stresses for which damage initiates through pure rocking is greater than the range where rocking determines the capacity. This is true for the shear mode as well. Conversely, the range of biaxial mode initiation is limited compared to the capacity envelope. Due to the usually low level of global vertical stress under which masonry piers typically operate in buildings [23], it is expected that the majority of piers will feature rocking or shearing damage initiation, followed by rocking, shearing or, less commonly, biaxial failure.

The damage initiation model is validated against a series of experiments carried out on piers at Delft University of Technology [24,25], coupled with extensive material characterisation [26,27]. The geometric and material parameters are reported in Table 1. The experiments include two different sets of materials, different masonry bonds, different boundary conditions and varying vertical pre-compression levels.

The damage initiation and final failure mode was reported in three of the cases (TUD_COMP_20, TUD_COMP_21, TUD_COMP_22), while for one of the cases (TUD_COMP_47/48) the crack pattern was objectively registered using digital image correlation (DIC). Systematic documentation and objective interpretation of damage initiation in experimental reports is often problematic without the use of DIC or other optical methods for crack tracking. Damage initiation is typically reported in terms of visible diagonal cracking, which cannot arise without prior initiation of some degree of rocking damage. Localised toe crushing may also be reported, but this phenomenon is associated with practically all damage initiation and capacity models and is, therefore, not indicative of the overall failure mode by itself. Nevertheless, even damage reported in simple terms can assist in interpreting damage initiation modes in masonry piers.

Table 1 Experimental case studies for pier model validation: geometric and material parameters. Force capacity prediction error in parentheses.

Parameter	Symbol	Unit	Case study			
Specimen name	-	-	TUD_COMP_20	TUD_COMP_21	TUD_COMP_22	TUD_COMP_47/48
Reference	-	-	[24]	[24]	[24]	[25]
Pier length	l	mm	1100	3070	3070	3070
Pier height	h	mm	2778	2710	2710	2710
Pier thickness	t	mm	102	100	210	100
Unit length	l_u	mm	214	210	210	210
Unit height	h_u	mm	72	50	50	50
Mortar bed joint height	h_m	mm	10	10	10	10
Unit compressive strength	f_{cu}	N/mm²	13.26	28.30	28.30	28.30
Mortar compressive strength	f_{cm}	N/mm²	7.57	3.81	3.81	3.81
Masonry compressive strength	f_c	N/mm²	6.35	14.02	10.67	11.35
Unit-mortar interface tensile strength	f_{ti}	N/mm²	0.12	0.15	0.15	0.09
Initial shear strength	f_v	N/mm²	0.13	0.12	0.12	0.14
Masonry bond	-	-	Running	Running	English	Running
Vertical stress	$-\sigma$	N/mm²	0.63	0.36	0.36	0.46
Boundary condition	-	-	Cantilever	Double-clamped	Cantilever	Cantilever
Damage initiation - experimental	-	-	Rocking	Shear/rocking	Rocking	Rocking
Failure mode – experimental	-	-	Rocking	Biaxial	Rocking	Biaxial
Shear force capacity – experimental	H_{exp}	kN	15.1	98.1	117.2	112.5
Damage initiation – model	-	-	Rocking	Rocking	Rocking	Rocking
Failure mode – model	-	-	Rocking	Biaxial	Rocking	Biaxial
Shear force capacity – model	H_{mod}	kN	13.5 (-10.6%)	100.6 (2.5%)	120.2 (2.6%)	106.2 (-5.6%)

Overall, the model exhibits very good accuracy in both capacity calculation and in predicting the damage initiation and failure mode. In cases TUD_COMP_21, TUD_COMP_22 and TUD_COMP_47/48 the model was able to predict the shift from a damage initiation mode based on rocking/sliding to a failure mode based on diagonal cracking. The number of suitable experimental cases suitable for validation of the proposed model, which need to include comprehensive material characterisation and unambiguous reporting of the damage initiation force and mode, is currently small, especially compared to the number of cases suitable for validation of the capacity model. Further experimental investigation focusing on damage initiation is thus motivated.

4 Strut & fan model for walls with openings

4.1 General model description

In the context of the proposed approach, modelling of masonry walls with openings under in-plane loads requires: 1) the discretisation of the frame into individual components, 2) the distribution of forces and stresses in these components, 3) the identification of potential failure modes according to the arrangement of the components and the boundary conditions.

The discretisation of a masonry wall with a single opening is shown in Figure 7, along with the notation used hereafter for dimensions and loads. The wall consists of 8 components arranged in a regular 3×3 grid. Three components for the spandrel (S_1, S_2 and S_3), two components for the piers (P_1 and P_3) and three components for the base (B_1, B_2 and B_3) are considered. The piers can have different lengths, thus allowing the analysis of asymmetric structures. Each component can be assigned its own thickness t and set of material properties. Additionally, the vertical load at the top of each pier and of the spandrel can be different. A height of $h_1 = 0$ reduces the model to a portal frame, while all the other dimensions can only be greater than 0. The horizontal loading direction is towards the positive of the x axis. Vertical compression is applied towards the negative of the y axis.

In the modular approach proposed, the wall W is composed of a pair of sub-systems: L (left) and R (right), connected with a central spandrel. Each sub-system consists of a single base, pier and spandrel. The capacity of the wall is dependent on the capacity of the individual sub-systems and the effect of their interaction through spandrel action.

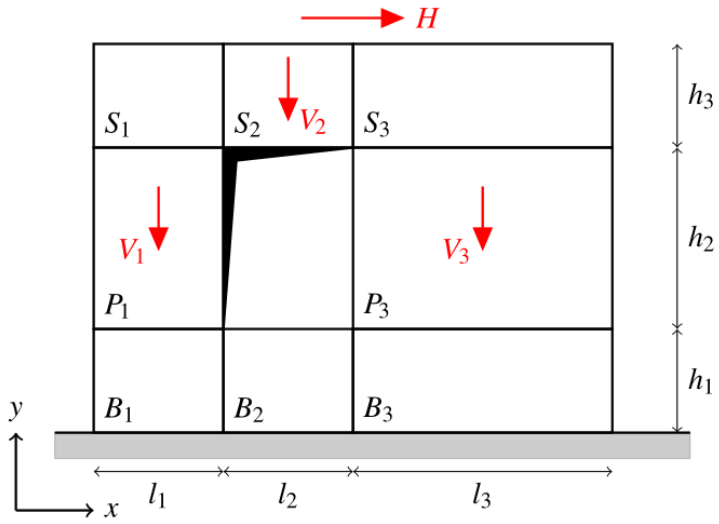

Figure 7 Discretisation of masonry wall with central opening into components.

4.2 Boundary conditions and spandrel function

As in the case of stand-alone piers, the wall is considered clamped at the base. For the boundary condition at the top, the wall may be in a) cantilever, b) clamped or c) clamped with vertical translational restraint configuration.

The boundary conditions and construction details at the top of the wall affect the function of the spandrel in providing frame action. In particular, for a cantilever configuration, two cases are distinguished: a) a "weak" connection with the piers, due to the absence of structural elements above the spandrel, and b) a "strong" connection with the piers, provided by steel or reinforced concrete capping beams or a strong lintel. In the former, the S_2 spandrel component responds to horizontal loading by "rocking" between the two piers: a hinge is formed at the top right corner of S_1 and another at the left bottom corner of S_3. In the latter case, the spandrel elements respond jointly. For the clamped and clamped with vertical restraint configurations, it is always considered that the spandrel provides a "strong" connection. The two types of spandrel function are illustrated in Figure 8.

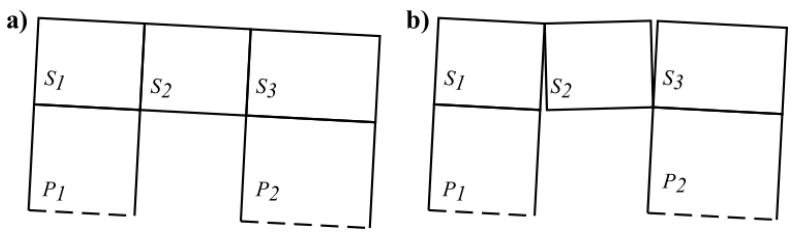

Figure 8 a) "Strong" and b) "weak" spandrel function under horizontal loading.

4.3 Modelling assumptions

The stress distribution in the components is represented through a system of compressive struts and fans. The compressive struts develop between two formed plastic hinges. Fans develop between two continuous lines of applied vertical displacement or between one such line and a plastic hinge.

Concerning the distribution of the compressive stresses, it is assumed that the vertical stress σ_1 is distributed to pier P_1, while both vertical stresses σ_2 and σ_3 are borne by pier P_3, due to the loading direction. The transfer of vertical load from the spandrel S_2 above the opening constitutes the frame action of the wall.

Plastic hinges are formed due to yielding in compression and have a width of b calculated as per the pier model through eq. (1).

4.4 Sub-system failure shapes

Eight arrangements of plastic hinges are possible for a sub-system, illustrated in Figure 9. Stress fans are depicted in light blue, with the direction of the stress flow indicated by arrows. Compressive struts are indicated in deeper blue colour. The expansion of the stress fan between hinges as expressed in eq. (10) and illustrated in Figure 2 is not shown for clarity of the illustrations. The plastic hinges are formed at the edges of the struts or at the convergence locus between a laterally contracting and an expanding stress fan.

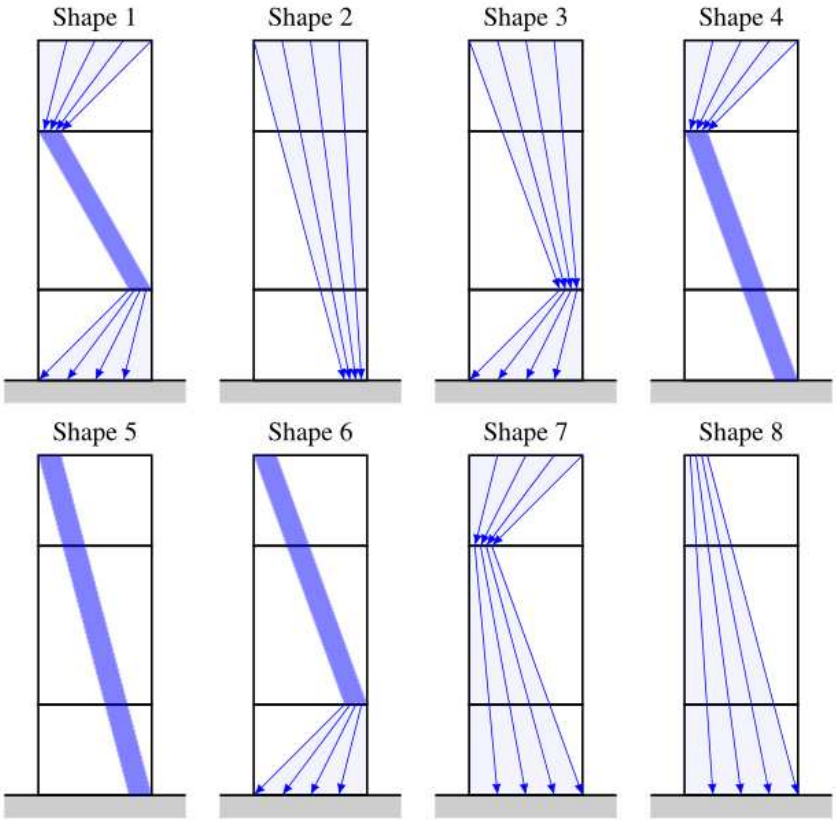

Figure 9 Potential failure shapes for base-pier-spandrel sub-system. Disposition of stress fans and compressive struts.

The disposition of the struts and fans determines where the failure checks are performed. This point is illustrated by commenting on the difference between shapes 1, 2 and 3. In shape 1, the spandrel, pier and base are checked individually. In shape 2 all three components are checked as one. In shape 3 the base is checked individually while the spandrel and pier are checked as one component.

Individual failure checks are executed according to the model for stand-alone piers: a) all components are checked against biaxial failure according to eq. (16), b) all components are checked in compression according to eq. (18), c) piers are checked in shear according to eq. (6), c) rocking failure is checked according to eq. (5) by calculating the horizontal force component between plastic hinges or, in the absence of a second plastic hinge, by assuming a resultant force at the centre of a fan extending towards the direction of loading (positive x direction).

The failure checks in sub-system L are straightforward due to the sub-system only bearing the vertical and horizontal forces applied on S_1. Sub-system B bears the vertical and horizontal forces applied on both

S_2 and S_3. For a "weak" spandrel, V_2 is transferred to the lower right corner of S_3, while for a "strong" spandrel it is applied at the centre of S_2, providing an increased lever-arm and increased rocking capacity. In the case of a "strong" spandrel, an additional biaxial strength check is performed for S_2, considering a stress fan from the top of S_2 to the top of P_2, where it assumes a width as defined in Figure 9.

Based on these calculations, the capacity $\tau_{A,i}$ and $\tau_{B,i}$ of each sub-system L or R for the failure shapes $i \in [1,8]$ is calculated.

4.5 Combination of sub-system failure shapes

The sub-system failure shapes are combined in pairs. Each pair defines a potential failure mode and total capacity for the wall. These capacity sums can be expressed as:

$$\boldsymbol{C}(i,j) = \left(\tau_{L,i} + \tau_{R,j}\right), \;\; i,j \in [1,8] \tag{23}$$

The capacity of the wall τ_W is defined as the minimum element in $\boldsymbol{C}$. However, due to their interaction in the wall and due to boundary conditions, not all sub-system failure shapes are allowed in the complete wall structure. The boundary conditions and geometry of the wall affect the stress distribution and potential failure modes as follows: a) cantilever wall with "weak" spandrel require the formation of 2 hinges, b) cantilever walls with "strong" spandrels require 3 hinges, c) hinges cannot form at the top of cantilever walls with "strong" spandrels for maintaining continuity of the applied vertical stress, d) double-clamped walls require 4 hinges, e) double-clamped walls with vertical restraint require 4 hinges, but the bending failure mode is inactivated, f) the central part B_2 of the base restricts the rotation of components B_1 and B_3 [28], therefore, no plastic hinge can form at the base of B_1 or B_3, unless a sufficient gap is provided between the base components.

Based on the above conditions, the allowable failure shape combinations are: a) $\boldsymbol{C}(3,3)$, $\boldsymbol{C}(3,7)$, $\boldsymbol{C}(3,8)$, $\boldsymbol{C}(7,3)$, $\boldsymbol{C}(7,7)$, $\boldsymbol{C}(7,8)$, $\boldsymbol{C}(8,7)$, and $\boldsymbol{C}(8,8)$ for a cantilever wall with a "weak" spandrel, b) $\boldsymbol{C}(1,3)$, $\boldsymbol{C}(3,1)$, $\boldsymbol{C}(1,7)$ and $\boldsymbol{C}(7,1)$ for a cantilever wall with a "strong" spandrel, c) $\boldsymbol{C}(1,1)$, $\boldsymbol{C}(1,6)$ and $\boldsymbol{C}(6,1)$ for the double-clamped, with or without vertical restraint.

4.6 Model results and validation

The proposed model for the masonry wall capacity is validated against experimental cases from the literature. Among the findings in the literature, the list of cases used was confined to those in which material parameters were reported. It includes both walls with window openings and portal frames, i.e. where $h_1 = 0$. Due to the small number of such available campaigns, nominal shear characteristics were assumed where they were missing in order to not overly limit the application cases [29]. The tensile strength as calculated according to eq. (17) and the friction angle of the masonry as calculated in subsection 2.4 are also reported. Concerning boundary conditions, walls were tested in cantilever with "strong" spandrel ('*C*') and double-clamped with vertical restraint ('*V*') configuration. The vertical load was only applied on the piers in a few instances. In one case of asymmetrical piers, the capacity in both positive and negative directions is reported (H_{exp}^{+} and H_{exp}^{-} respectively). The parameters used and the comparison of the experimental and model results are presented in Table 2. In addition to calculating the model capacity H_{mod}^{+} in the positive direction, the capacity in the negative direction H_{mod}^{-} was calculated by reversing the parameters l_1 and l_3. Overall a very good prediction of the experimental capacity is obtained using the proposed model for this wide variety of experimental cases.

The difference in wall capacity due to uneven piers, accompanied by a shift in failure mode, is captured in the simulation of the experiments by Esposito & Ravenshorst [24]. The quarter-scale experiments by Lobato [30] and full-scale experiments by Foraboschi & Vanin [13,31] illustrate the shift in capacity due to an increasing vertical load, an increase indicative of the global friction angle of the masonry. The accuracy of the model in simulating large piers connected by a spandrel, namely portal frames without the base, is shown in the simulation of the experiments by Parisi et al [14]. Finally, the model captures the significant effect of boundary conditions on the response, as illustrated in the high capacity obtained in the experiments by Raijmaker, which was vertically restrained, resulting in a force capacity nearly double that of a double-clamped model [12].

Table 2 Comparison of wall with opening capacity model with experimental results from the literature. Predicted force error in parentheses.

Ref.	h_1	h_2	h_3	l_1	l_2	l_3	t	f_c	f_v	μ	f_t	$-\sigma$	Boundary conditions	Masonry bond	H^+_{exp}	H^+_{mod}	H^-_{exp}	H^-_{mod}
–	mm	mm	mm	mm	mm	mm	mm	N/mm²	N/mm²	–	N/mm²	N/mm²	–	–	kN	kN	kN	kN
[30]	90	90	90	150	75	112.5	35	18.9	0.46	2.42	1.70	0.645	*C*	Running	4.9	5.7 (16.3%)	-	-
												1.132			7.7	9.6 (24.7%)	-	-
												1.858			13.1	12.5 (-4.6%)	-	-
												2.540			13.2	14.5 (9.8%)	-	-
												3.236			15.9	16.3 (2.5%)	-	-
												4.036			17.7	17.9 (1.1%)	-	-
[14]	0	2300	1000	1700	1700	1700	310	3.73	0.15	1.36	0.26	0.373[b]	*C*	Running	184	171.5 (-6.8%)	-	-
[31]	325	1170	845	930	880	930	240	1.21	0.15[a]	2.36	0.16	0.300[b]	*C*	Flemish	63	51.7 (-17.9%)	-	-
												0.179[b]			48	37.8 (-21.3%)	-	-
												0.090[b]			18	19.4 (7.7%)	-	-
[13]	380	1210	1180	1025	1070	1025	250	1.21	0.15[a]	2.64	0.16	0.270[b]	*C*	Flemish	64.2	60.4 (-5.9%)	-	-
												0.179[b]			59.8	43.2 (-27.8%)	-	-
												0.090[b]			18.2	24.4 (34.1%)	-	-
[25]	530	1510	650	870	780	1420	100	11.35	0.13	1.75	0.37	0.120	*C*	Running	22.2	19.3 (-13.1%)	-	-
[24]	540	1680	490	870	1000	1200	210	10.67	0.2	0.88	0.32	0.340	*C*	English	85.4	84.2 (-1.4%)	94.1	90.4 (-3.9%)
[12]	350	350	350	430	210	325	100	10.5	0.35	1.75	0.66	0.300	*V*	Running	41.5	45.6 (9.9%)	-	-

[a] assumed value

[b] vertical load applied over pillars only

5 Conclusions

An analytical model for the prediction of the in-plane capacity of masonry piers and walls with openings is presented. The model considers all major geometric and material parameters, including the bond type, for the calculation of the capacity. Additionally, an analytical model is proposed for the prediction of the damage initiation mode in masonry piers under in-plane shear. Apart from geometric and material properties, no further numerical parameters or major empirical assumptions are needed for analysis.

The model accounts for all potential failure modes normally encountered in masonry walls subjected to a combination of in-plane vertical and horizontal loading. Unequal vertical loading, asymmetric piers and local variations in material properties can be easily introduced in the analysis.

The basis of the model is validated against numerous standalone pier experimental tests, while the model for walls with openings is similarly validated against several case studies with different material properties, dimensions, bonding patterns and boundary conditions.

The model provides a very efficient and accurate method for the capacity assessment of simple structures subjected to in-plane shear loading under vertical stress. The damage initiation model provides a simple means of highlighting weaknesses in masonry piers, thus allowing efficient intervention design for the strengthening of masonry structures against damage initiation.

The proposed model presents opportunities for future work pertaining to the simulation of structural reinforcement, such as in the form of embedded bars. The contribution of horizontal bars can be introduced in the tensile strength for the biaxial failure check. Vertical bars can increase the rocking mode capacity when anchored at the base of cantilever walls, or at the base and top of double-clamped piers. Finally, diagonal bars can restore or increase the cohesion in damaged zones.

References

[1] Magenes G, Calvi GM. In-plane seismic response of brick masonry walls. Earthq Eng Struct Dyn 1997;26:1091–112. https://doi.org/10.1002/(SICI)1096-9845(199711)26:11<1091::AID-EQE693>3.0.CO;2-6.

[2] Roca P, Viviescas Jaimes Á, Lobato Paz EM, Díaz C, Serra I. Capacity of shear walls by simple equilibrium models. Int J Archit Herit 2011;5:412–35. https://doi.org/10.1080/15583058.2010.501481.

[3] Ministerio delle Infrastrutture e dei Trasporti. Circolare 2 febbraio 2009, n. 617 Istruzioni per l'applicazione delle "Nuove norme tecniche per le costruzioni" di cui al decreto ministeriale 14 gennaio 2008. 2009.

[4] Tomaževič M. Earthquake-Resistant Design of Masonry Buildings. London: Imperial College Press; 2006.

[5] CEN. EN 1996-1-1 - Eurocode 6 - Design of masonry structures - Part 1-1: General rules for reinforced and unreinforced masonry structures. 2005.

[6] Mann W, Muller H. Failure of Shear-Stressed Masonry. An Enlarged Theory, Tests and Application to Shear Walls. Proc. Br. Ceram. Soc., 1982, p. 223–35.

[7] Turnšek V, Cacovic F. Some experimental results on the strength of brick masonry walls. Proc. 2nd Intern. Brick Mason. Conf., 1971, p. 149–56.

[8] Turnšek V, Sheppard P. The shear and flexural resistance of masonry walls. Int. Res. Conf. Earthq. Eng., 1980.

[9] Beyer K. Peak and residual strengths of brick masonry spandrels. Eng Struct 2012;41:533–47. https://doi.org/10.1016/j.engstruct.2012.03.015.

[10] Morandi P, Albanesi L, Graziotti F, Li Piani T, Penna A, Magenes G. Development of a dataset on the in-plane experimental response of URM piers with bricks and blocks. Constr Build Mater 2018;190:593–611. https://doi.org/10.1016/j.conbuildmat.2018.09.070.

[11] Messali F, Esposito R, Ravenshorst G. JP, Rots JG. Experimental investigation of the in-plane cyclic behaviour of calcium silicate brick masonry walls. vol. 18. Springer Netherlands; 2020. https://doi.org/10.1007/s10518-020-00835-x.

[12] Raijmaker TM., Vermeltfoort AT. Deformation controlled meso shear tests on masonry piers. Rep. B-

92-1156, TNO- BOUW/TU Eindhoven. TNO- BOUW/TU Eindhoven; 1992.

[13] Foraboschi P. Coupling effect between masonry spandrels and piers. Mater Struct 2009;42:279–300. https://doi.org/10.1617/s11527-008-9405-7.

[14] Parisi F, Augenti N, Prota A. Implications of the spandrel type on the lateral behavior of unreinforced masonry walls. Earthq Eng Struct Dyn 2014;43:1867–87. https://doi.org/10.1002/eqe.2441.

[15] Drougkas A, Roca P, Molins C. Experimental Analysis and Detailed Micro-Modeling of Masonry Walls Subjected to In-Plane Shear. Eng Fail Anal 2019;95:82–95. https://doi.org/10.1016/j.engfailanal.2018.08.030.

[16] Korswagen PA, Longo M, Meulman E, Rots JG. Crack initiation and propagation in unreinforced masonry specimens subjected to repeated in-plane loading during light damage. Bull Earthq Eng 2019;17:4651–87. https://doi.org/10.1007/s10518-018-00553-5.

[17] Van Staalduinen P, Terwel K, Rots JG. Onderzoek naar de oorzaken van bouwkundige schade in Groningen Methodologie en case studies ter duiding van de oorzaken. Report number: CM-2018-01. TU Delft; 2018.

[18] Terwel K, Schipper R. Innovative ways of dealing with existing problems: How to reliably assess the cause of damage of masonry structures in an area with man-induced earthquakes? IABSE Symp. Nantes 2018 Tomorrow's Megastructures, 2018, p. S23-39-S23-46.

[19] Drougkas A, Licciardello L, Rots JG, Esposito R. In-plane seismic behaviour of retrofitted masonry walls subjected to subsidence-induced damage. Eng Struct 2020;223:111192. https://doi.org/10.1016/j.engstruct.2020.111192.

[20] Beer FP, Johnston ER, DeWolf JT, Mazurek DF. Mechanics of Materials. New York: McGraw-Hill Professional; 2012.

[21] Drougkas A, Roca P, Molins C. Numerical prediction of the behavior, strength and elasticity of masonry in compression. Eng Struct 2015;90:15–28. https://doi.org/10.1016/j.engstruct.2015.02.011.

[22] Timoshenko S. Strength Of Materials. D. Van Nostrand Company; 1940.

[23] Heyman J. The stone skeleton. Int J Solids Struct 1966;2:249–79. https://doi.org/10.1016/0020-7683(66)90018-7.

[24] Esposito R, Ravenshorst G. JP. Quasi-static cyclic in-plane tests on masonry components 2016/2017. Report number: C31B67WP3-4. TU Delft; 2017.

[25] Korswagen PA, Longo M, Meulman E, van Hoogdalem C. Damage sensitivity of Groningen masonry structures - Experimental and computational studies. Report number: C31B69WP0-11. TU Delft; 2017.

[26] Jafari S, Esposito R. Material tests for the characterisation of replicated solid calcium silicate brick masonry. Report number: C31B67WP1-9. TU Delft; 2016.

[27] Jafari S, Esposito R. Material tests for the characterisation of replicated solid clay brick masonry. Report number: C31B67WP1-12. TU Delft; 2017.

[28] Caliò I, Marletta M, Pantò B. A new discrete element model for the evaluation of the seismic behaviour of unreinforced masonry buildings. Eng Struct 2012;40:327–38. https://doi.org/10.1016/j.engstruct.2012.02.039.

[29] Van der Pluijm R. Material properties of masonry and its components under tension and shear. 6th Can. Mason. Symp. Saskatoon, 1992, p. 675–86.

[30] Lobato Paz EM. Método simple para el análisis de muros de obra de fábrica con aberturas bajo solicitaciones en su plano. PhD dissertation. 2009.

[31] Vanin A, Foraboschi P. In-plane behavior of perforated brick masonry walls. Mater Struct 2012;45:1019–34. https://doi.org/10.1617/s11527-011-9814-x.

List of Figures

List of Tables